ORIGINAL ARTICLE

Cancer Science WILEY

RPV-modified epirubicin and dioscin co-delivery liposomes suppress non-small cell lung cancer growth by limiting nutrition supply

Liang Kong[1] | Fu-yi Cai[1] | Xue-min Yao[1] | Ming Jing[1] | Min Fu[1] | Jing-jing Liu[1] |
Si-yu He[1] | Lu Zhang[1] | Xin-ze Liu[1] | Rui-jun Ju[2] | Xue-tao Li[1] (iD)

[1]School of Pharmacy, Liaoning University of Traditional Chinese Medicine, Dalian, China

[2]Department of Pharmaceutical Engineering, Beijing Institute of Petrochemical Technology, Beijing, China

Correspondence
Rui-jun Ju, Department of Pharmaceutical Engineering, Beijing Institute of Petrochemical Technology, Beijing, China.
Email: juruijun@bipt.edu.cn

Xue-tao Li, School of Pharmacy, Liaoning University of Traditional Chinese Medicine, Dalian, China.
Email: lixuetao1979@163.com

Abstract

Chemotherapy for non-small cell lung cancer (NSCLC) is far from satisfactory, mainly due to poor targeting of antitumor drugs and self-adaptations of the tumors. Angiogenesis, vasculogenic mimicry (VM) channels, migration, and invasion are the main ways for tumors to obtain nutrition. Herein, RPV-modified epirubicin and dioscin co-delivery liposomes were successfully prepared. These liposomes showed ideal physicochemical properties, enhanced tumor targeting and accumulation in tumor sites, and inhibited VM channel formation, tumor angiogenesis, migration and invasion. The liposomes also downregulated VM-related and angiogenesis-related proteins in vitro. Furthermore, when tested in vivo, the targeted co-delivery liposomes increased selective accumulation of drugs in tumor sites and showed extended stability in blood circulation. In conclusion, RPV-modified epirubicin and dioscin co-delivery liposomes showed strong antitumor efficacy in vivo and could thus be considered a promising strategy for NSCLC treatment.

KEYWORDS
angiogenesis, cell-penetrating peptide, co-delivery liposome, non-small cell lung cancer, vasculogenic mimicry

1 | INTRODUCTION

Lung cancer is one of the most common malignancies and a leading cause of cancer-related death worldwide.[1] Among all lung cancers, approximately 85% are non-small cell lung cancer (NSCLC), for which morbidity is significantly higher than for small cell lung cancer.[2] In the past decade, targeted therapy, immunotherapy, and similar approaches rapidly developed to become the new treatment modalities for NSCLC. Despite recent developments and improvements in diagnosis and treatment, prospects for patients with NSCLC are dismal and the 5-year overall survival rate is only 15%-18%.[3,4] Rapid growth and metastasis are basic biological characteristics of malignant tumors, including NSCLC.[5] It is well known that angiogenesis plays a key role in cancer growth and metastasis. Anti-angiogenesis treatment has evolved to achieve encouraging results, but despite the widespread application of anti-angiogenic drugs, they have not attained satisfactory efficacy.[6-8] This means that alternative nutrient supply channels support tumor growth.

Vasculogenic mimicry (VM) is defined as formation of vascular-like structures lined with tumor cells without the presence

of endothelial cells.[9] VM has been found in a variety of invasive cancers, including NSCLC, colorectal, breast, melanoma, and head and neck squamous cell carcinomas.[10-14] As a newly defined mechanism providing oxygen and nutrients to tumor tissues, extensive VM has been identified as an important risk factor, indicating poor prognosis, low survival, and high invasiveness and metastasis in cancer patients.[15] Formation of VM channels is related to a series of extracellular matrix remodeling factors, such as vascular endothelial cadherin (VE-Cad), MMP, hypoxia inducible factor 1-alpha (HIF-1α), and vascular endothelial growth factor A (VEGFA).[16,17]

As an isomer of doxorubicin, epirubicin is an anthracycline anticancer drug, showing lower toxicity than doxorubicin. It has been widely used as a base for single or combination chemotherapy treatment for solid tumors, including NSCLC.[18-20] However, free epirubicin shows poor tumor selectivity and hence can cause significant side-effects, such as myelosuppression, cardiotoxicity, and allergic reactions.[21] Emergence of novel drug carriers can compensate for these disadvantages of the free (without carrier) drugs. Liposomes, which have strong affinity to cell biofilms, are commonly used carriers for antitumor drugs and can act as new targeting vectors for free drugs.[22,23]

Dioscin ($C_{45}H_{72}O_{16}$, 869.05 Da) is a natural product, isolated from medicinal plants such as *Dioscorea nipponica* and *Paridis* rhizome.[24] Dioscin has attracted considerable attention because of its broad-spectrum pharmacological functions, including anti-inflammatory,

antiviral, anti-obesity and anti-fungal activities.[25,26] Furthermore, the potential antitumor effects of dioscin have been confirmed in various cancer cells, including human lung cancer A549 cells, and human leukemia K562 and HL60 cells.[27] Moreover, dioscin can inhibit transforming growth factor-beta (TGF-β)1-induced migration and invasion of A549 lung cancer cells, as well as tumor growth and angiogenesis in colon cancer C26 cell-derived tumor in mice.[28,29]

In recent years, cell penetrating peptides (CPPs) have been widely used as motifs for delivering drugs to tumors. CPPs are short peptides that can be anchored onto the surface of carriers (eg, liposomes) for efficiently delivering the carriers into tumor cells.[30] CPPs were initially discovered when studying the short sequences of membrane-interacting proteins known as protein transduction domains (PTD). These peptide sequences are cationic, hydrophobic, and/or amphipathic in nature.[31,32] RPV peptide (RGDPFVYLI) is a novel small-molecule cell-penetrating peptide that can enhance drug uptake in tumor cells.

The present study investigated the synergistic antitumor effects of RPV-modified targeted liposomes incorporated with both epirubicin and dioscin. In the targeted liposomes, RPV was incorporated onto the liposomal surface to enhance cellular uptake. Dioscin was encapsulated inside the lipid bilayer and used as a regulator to inhibit tumor metastasis, neovascularization, and formation of VM channels. Epirubicin was loaded into the hydrophilic inner core of the liposomes as a cytotoxic drug. The aim of the present study was to develop novel
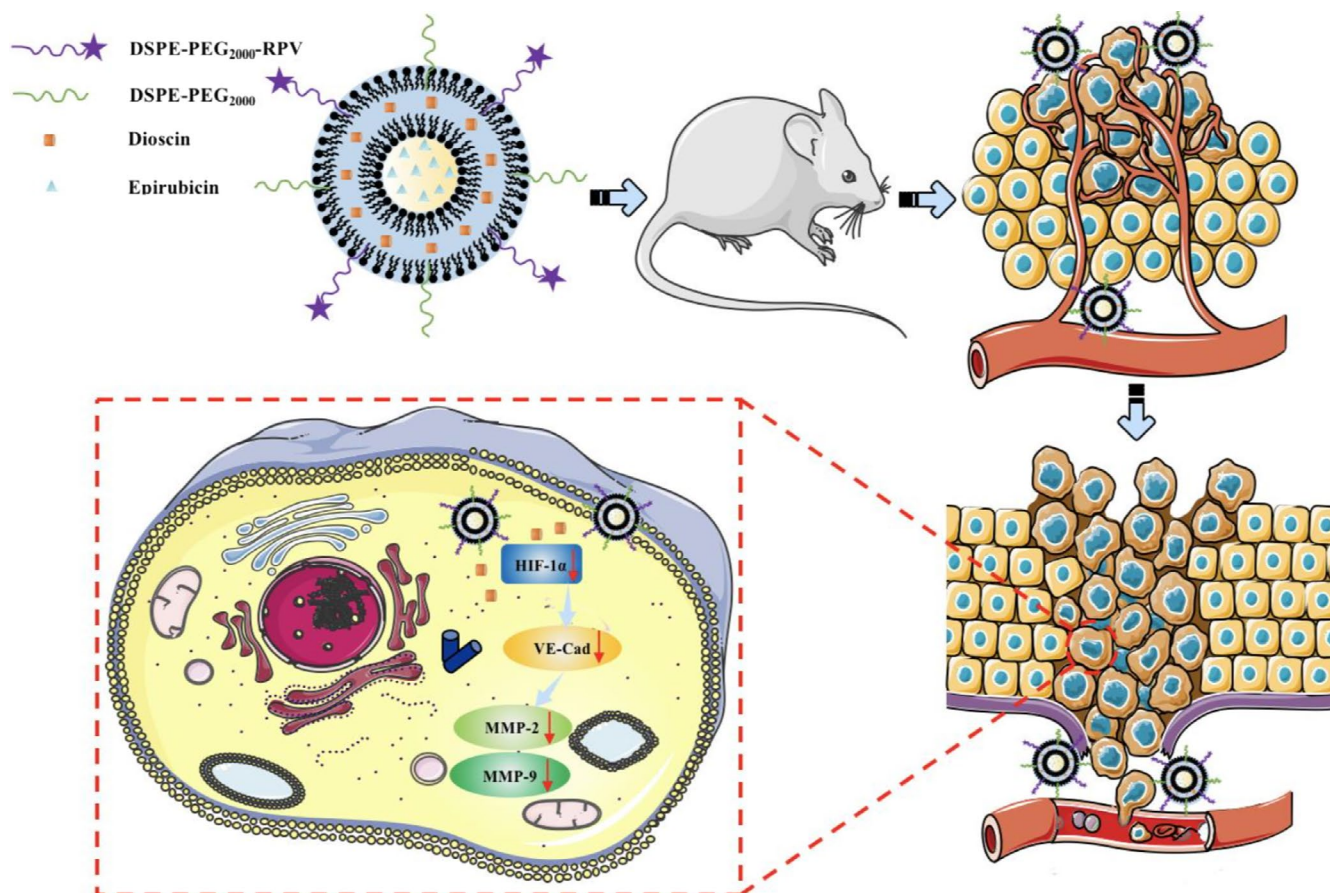
FIGURE 1 Schematic illustration of the strategy behind the use of RPV-modified epirubicin and dioscin co-delivery liposomes for non-small cell lung cancer treatment. HIF-1α, hypoxia-inducible factor 1 alpha; VE-Cad, vascular endothelial cadherin
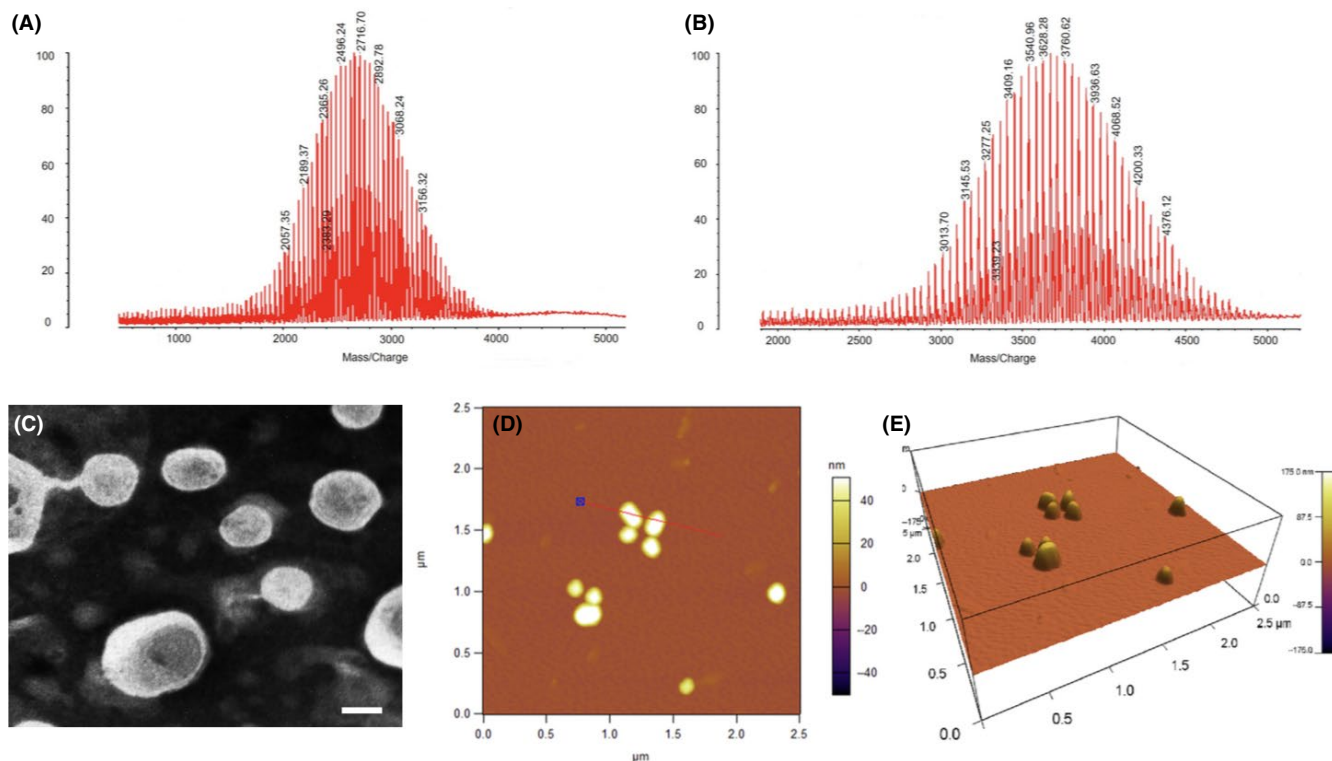
FIGURE 2 Characterization of RPV-modified epirubicin and dioscin co-delivery liposomes. A, MALDI/ionization time-of-flight mass spectroscopy (MALDI-TOF-MS) spectrum of DSPE-PEG$_{2000}$-COOH. B, MALDI-TOF-MS spectrum of DSPE-PEG$_{2000}$-RPV. C, Transmission electron microscopy (TEM) image of RPV-modified epirubicin and dioscin co-delivery liposomes. Scale bar, 20 nm. D, Atomic force microscopy image of RPV-modified epirubicin and dioscin co-delivery liposomes. E, 3-D reconstruction of (D)

targeted liposomes, and explore their antitumor effects on NSCLC, as well as to elucidate possible mechanisms of action (Figure 1).

2 | MATERIALS AND METHODS

2.1 | Cells and animals

Human NSCLC A549 cells were purchased from the Institute of Basic Medical Science, Chinese Academy of Medical Science. Cells were cultured in RPMI-1640 culture medium supplemented with 10% FBS (EallBio), 100 U/mL penicillin and 100 µg/mL streptomycin at 37°C in humidified atmosphere of 5% CO_2 in air. Male BALB/c nude mice, weighing 20 ± 2 g, were obtained from the Peking University Experimental Animal Center. Sprague-Dawley (SD) rats were purchased from Liaoning Changsheng Biotechnology Co., Ltd. This research was approved by the Institutional Authority for Laboratory Animal Care of Peking University.

2.2 | Synthesis of DSPE-PEG$_{2000}$-RPV

The targeted molecule of 2-distearoyl-*sn*-glycero-3-phosphoethanol-amine-*N*-methoxy-poly(ethylene glycol 2000)-RPV (DSPE-PEG$_{2000}$-RPV) was synthesized by binding DSPE-PEG$_{2000}$-COOH and the RPV peptide, following a previously reported protocol.[33] Briefly,

DSPE-PEG$_{2000}$-COOH and RPV peptide (1:1 molar ratio) were dissolved in anhydrous dimethylformamide. Reaction pH was adjusted to pH 9.0 with N-methylmorpholine. The solution was stirred overnight at room temperature, and then dialyzed overnight using 3-kDa molecular weight cutoff (MWCO) dialysis tubing to remove unbound material. Subsequently, the solution was lyophilized and stored at −20°C. The DSPE-PEG$_{2000}$-RPV product was then characterized by MALDI/ionization time-of-flight mass spectrometry (MALDI-TOF-MS).

2.3 | Preparation of liposomes

RPV-modified epirubicin and dioscin co-delivery liposomes were prepared using thin-film hydration.[34] Briefly, egg-yolk phosphatidylcholine (EPC), cholesterol, DSPE-PEG$_{2000}$, DSPE-PEG$_{2000}$-RPV, and dioscin were dissolved in methyl alcohol at a molar ratio of 100:30:3:2:7 in a pear-shaped bottle, and dried by rotary evaporator at 37°C to obtain a thin film. The thin film was hydrated with 5 mL ammonium sulfate and sonicated in a water bath. The suspension was then sonicated in an ice bath with a probe sonicator for 10 minutes at 200 W. Subsequently, the samples were extruded three times through a polycarbonate membrane with 200 nm pores to obtain the RPV-modified dioscin liposomes. These were transferred to a cellulose ester membrane (1.2-1.4 kDa MWCO) for dialysis in triplicate with PBS. After dialysis, to prepare the RPV-modified epirubicin and dioscin co-delivery

liposomes, epirubicin was encapsulated (EPC: epirubicin molar ratio of 100:7) in a water bath at 40°C with shaking for 20 min. In addition, epirubicin and dioscin co-delivery liposomes, epirubicin liposomes, dioscin liposomes, and blank liposomes were also prepared by the same processes as above, adding DSPE-PEG$_{2000}$-RPV, dioscin, or epirubicin. Liposomes loaded with 1,10-dioctadecyl-3,3,30,30-tetramethylindotricarbocyanine (DiR) were also prepared by the same procedure, but the drug was replaced with a fluorescent probe (EPC: DiR, 200:1, w/w).

2.4 | Characterization of liposomes

Particle size, polydispersity index, and zeta potential values of all liposome types were determined using dynamic light scattering in a Zetasizer Nano ZS90 instrument (Malvern Instruments). Liposome morphology was studied using transmission electron microscopy (TEM, JEM-1200EX; JEOL) and atomic force microscopy (AFM, Cypher; Asylum Research Inc.). Liposome content of epirubicin and dioscin was measured using HPLC with an ultraviolet detector (LC-2010AHT; Shimadzu). Unencapsulated drug was removed by elution using a Sephadex G-50 column. Encapsulation efficiencies (EE) were calculated using the following equation: EE% = ($W_{encapsulated}$/W_{total}) × 100%, where $W_{encapsulated}$ and W_{total} represent the amount of drugs in liposomes and the total amount of drugs, respectively.[35,36]

Additional materials and methods are described in Document S1.

3 | RESULTS

3.1 | Characterization of the target molecule and liposomes

We characterized the target molecule using MALDI-TOF-MS, and the results are presented in Figure 2A,B. Average mass of DSPE-PEG$_{2000}$-COOH and DSPE-PEG$_{2000}$-RPV was 2716.70 (Figure 2A) and 3766.62 (Figure 2B), respectively. According to the MALDI-TOF-MS spectrum, the mass difference between the two molecules corresponded to the mass of the RPV peptide, confirming the successful synthesis of DSPE-PEG$_{2000}$-RPV. Characteristics of RPV-modified epirubicin and dioscin co-delivery liposomes

can be clearly observed in Figure 2C-E. TEM (Figure 2C) and AFM (Figure 2D, 2) images show that RPV-modified epirubicin and dioscin co-delivery liposomes are spherical in shape, having a smooth surface, and a diameter of approximately 100 nm with a narrow polydispersity index (≤0.20). Physical properties such as particle size, polydispersity index (PDI), zeta potential, and encapsulation efficiency are presented in Table 1. Encapsulation efficiencies of epirubicin and dioscin were above 90% for all liposomes.

3.2 | Cellular uptake and targeted effects in vitro

Results of qualitative and quantitative analyses of A549 cell uptake of RPV-modified epirubicin and dioscin co-delivery liposomes are shown in Figure 3. Quantitative evaluation by flow cytometry showed that the order of fluorescence intensity was in the following sequence: free epirubicin >RPV-modified epirubicin and dioscin co-delivery liposomes >epirubicin and dioscin co-delivery liposomes ≥epirubicin liposomes (Figure 3A,B). Results indicate that the addition of RPV peptide can significantly increase the uptake of drugs by A549 cells. As shown in Figure 3C,D, cellular uptake of RPV-modified epirubicin and dioscin co-delivery liposomes progressively increased over time. We also observed intracellular targeting effects by fluorescence epirubicin-specific staining. As can be noted in Figure 3E, the intracellular fluorescence intensity of RPV-modified epirubicin and dioscin co-delivery liposomes was higher than that of other liposomes. Furthermore, the highest uptake was found to be of free epirubicin as a result of direct contact between drug molecules and cell membranes, and their diffusion into cells. In order to more clearly observe liposome localization in cells, laser scanning confocal microscopy was used. A strong fluorescence signal was observed in the cellular membrane and the nuclei of A549 cells after incubation with RPV-modified epirubicin and dioscin co-delivery liposomes.

3.3 | Cytotoxic effects

Cytotoxic effects of the free drugs on A549 cells are shown in Figure 4A. Results show that at concentrations of up to 5 μmol/L, dioscin had little cytotoxicity against A549 cells. However, free epirubicin showed significant cytotoxicity in

**TABLE 1** Particle size, zeta potential and encapsulation efficiency of liposomes (n = 3)

Liposome	Size (nm)	PDI	Zeta (mV)	EE % Epirubicin	Dioscin
Blank liposomes	91.45 ± 2.17	0.166 ± 0.002	−6.44 ± 0.67	—	—
Dioscin liposomes	98.36 ± 1.79	0.174 ± 0.003	−5.73 ± 0.49	—	94.14 ± 3.19
Epirubicin liposomes	95.72 ± 1.88	0.185 ± 0.009	−7.12 ± 0.86	91.27 ± 2.59	—
Epirubicin and dioscin co-delivery liposomes	112.39 ± 3.03	0.177 ± 0.011	−5.91 ± 0.25	93.44 ± 3.15	91.27 ± 4.16
RPV-modified epirubicin and dioscin co-delivery liposomes	124.25 ± 2.46	0.183 ± 0.023	−6.38 ± 0.53	93.30 ± 2.88	92.48 ± 3.74

"–" Means the liposome does not need to evaluate this data.
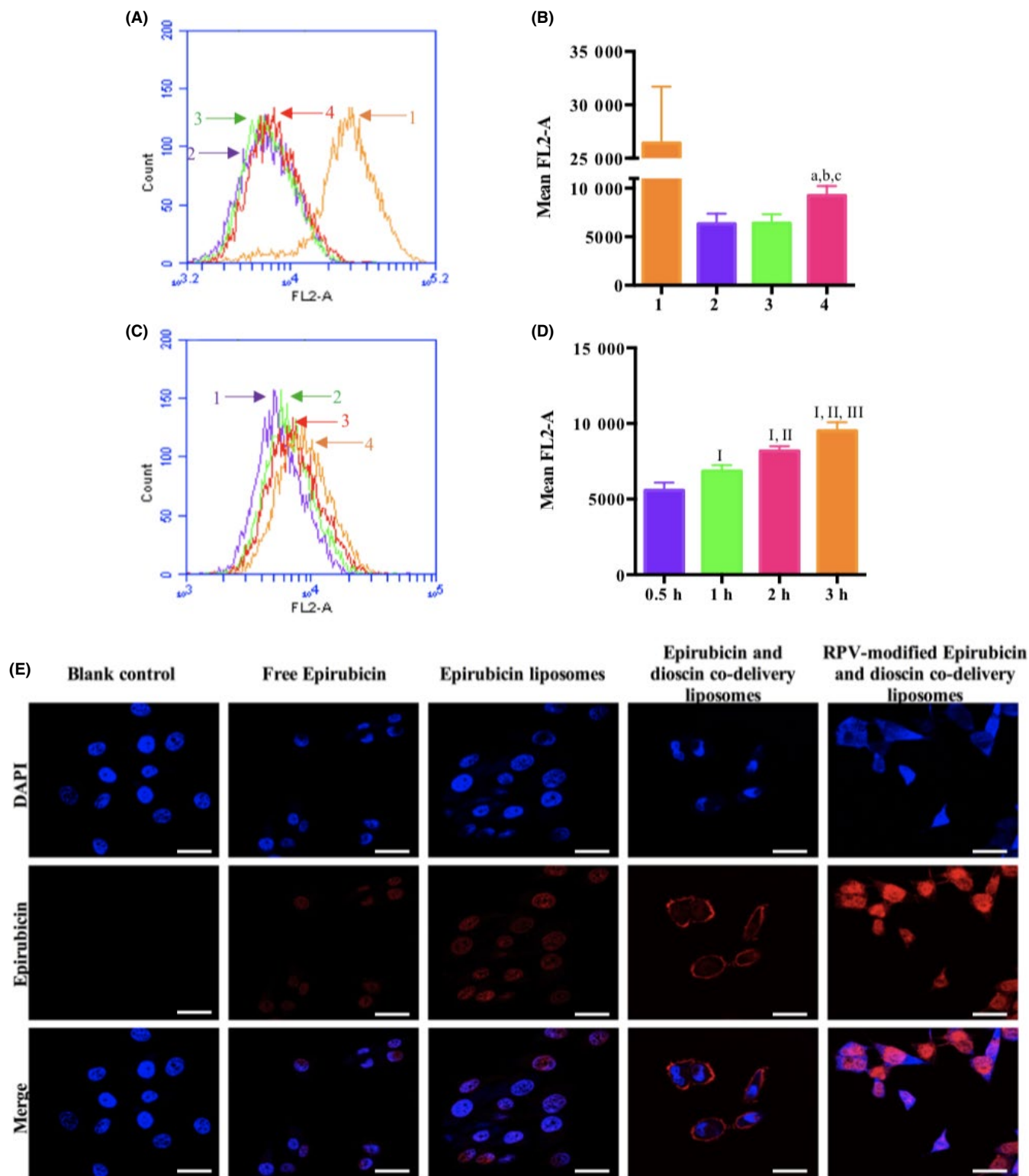
FIGURE 3 Cellular uptake and distribution after incubation with various liposomal formulations. A, Cellular uptake in A549 cells treated with the various liposomal formulations or free epirubicin. B, Quantitative analysis of fluorescence intensity. 1. Free epirubicin; 2. epirubicin liposomes; 3. epirubicin and dioscin co-delivery liposomes; 4. RPV-modified epirubicin and dioscin co-delivery liposomes. Data are presented as mean ± SD (n = 3). Comparison of a vs 1, b vs 2, and c vs 3. Significance level was set at $P < .05$. C, Cellular uptake in A549 cells treated with RPV-modified epirubicin and dioscin co-delivery liposomes at different time points. D, Quantitative analysis of fluorescence intensity; Data are presented as mean ± SD (n = 3). Comparison of I vs 0.5 h, II vs 1 h, and III vs 1.5 h. Significance level was set at $P < .05$. E, Cellular uptake and accumulation of liposomes in the nuclei of A549 cells incubated with the various formulations. Assessment was done by confocal fluorescence microscopy. Scale bar, 25 μm (n = 3)
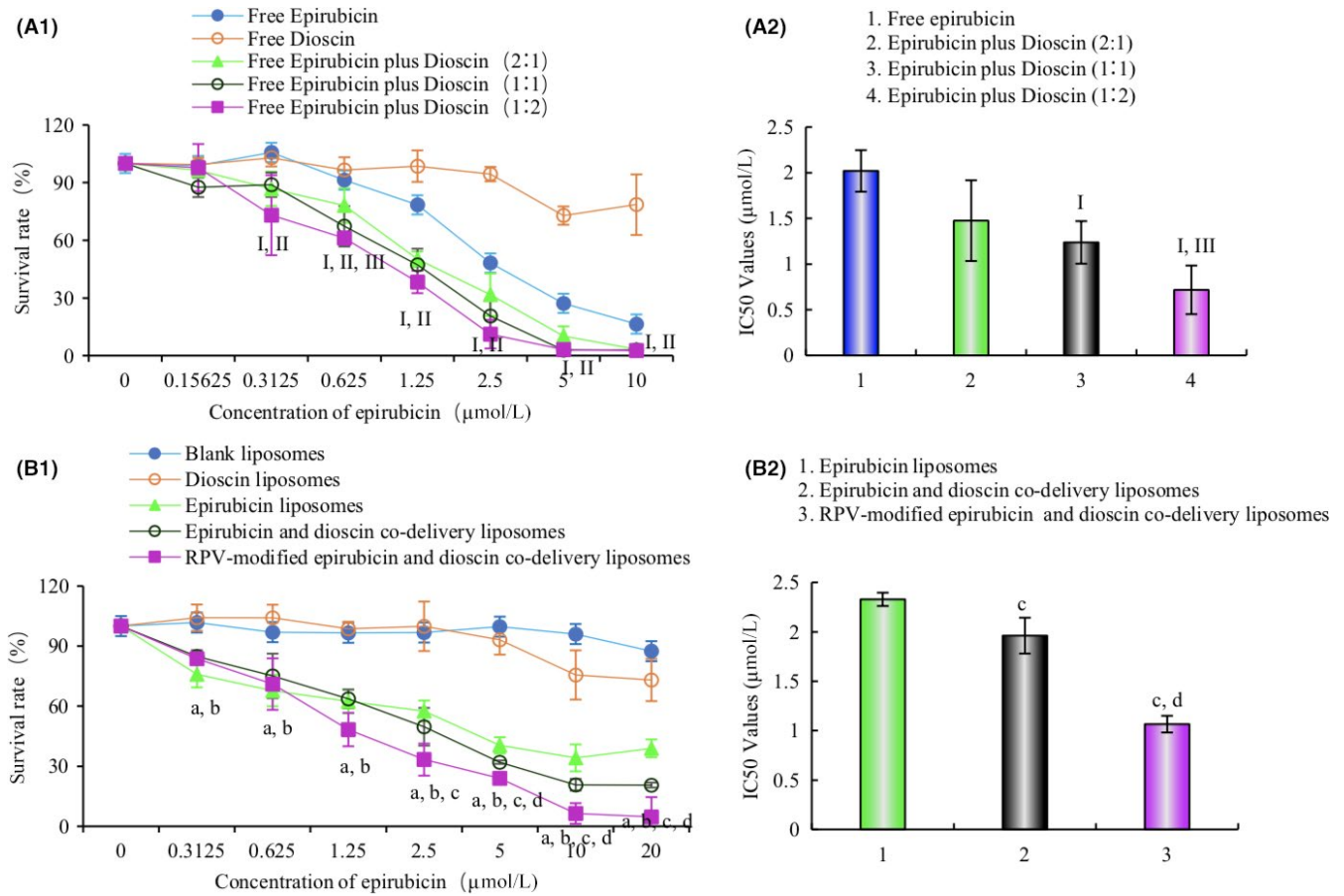
FIGURE 4 Inhibitory effects on A549 cells after treatment with various liposomal formulations. A, Inhibitory effects of free drugs. I vs free epirubicin, II vs free dioscin, III vs free epirubicin plus dioscin (molar ratio of 1:2). B, Inhibitory effects of liposomal formulations. Comparison of a vs blank liposomes, b vs dioscin liposomes, c vs epirubicin liposomes, d vs epirubicin and dioscin co-delivery liposomes. Data are presented as mean ± SD (n = 6). A1 is inhibitory effects of free drugs; A2 is statistical analysis of IC50 value of free drugs; B1 is inhibitory effects of liposomal formulations; B2 is statistical analysis of IC50 value of liposomal formulations. Significance level set at $P < .05$

a dose-dependent method. Moreover, the cytotoxic effect of free epirubicin was further enhanced by the addition of different concentrations of dioscin (molar ratios of 1:1, 1:2, and 2:1). At a 1:1 molar ratio between the drugs, IC_{50} value was 1.24 ± 0.23 μmol/L, considerably lower than that of free epirubicin (2.02 ± 0.23 μmol/L). Cytotoxic effects of liposomal formulations on A549 cells are presented in Figure 4B. Results show that blank liposomes had negligible cytotoxic effect, and dioscin liposomes showed little cytotoxicity within the range of 0-10 μmol/L. Among all liposomes, RPV-modified epirubicin and dioscin co-delivery liposomes showed the strongest cytotoxicity. IC_{50} values for epirubicin liposomes, epirubicin and dioscin co-delivery liposomes, and RPV-modified epirubicin and

dioscin co-delivery liposomes were 2.32 ± 0.07, 1.96 ± 0.18, and 1.06 ± 0.08 μmol/L, respectively.

3.4 | Inhibition of VM formation in vitro

As shown in Figure 5A, vascular-like structures were observed near A549 cells on the matrix gel when treated with blank liposomes control. However, a significant decrease in tube formation was observed when the A549 cells were incubated with dioscin-loaded liposomal formulations, where RPV-modified epirubicin and dioscin co-delivery liposomes showed the strongest inhibitory effect. Epirubicin liposomes also showed a slight damaging effect

FIGURE 5 Inhibitory effects on vasculogenic mimicry (VM) channel formation and angiogenesis after treatment with various liposomal formulations. A, Inhibition of VM channel formation. Scale bar, 50 μm. B, Representative bands of the proteins MMP-2, MMP-9, hypoxia-inducible factor 1 alpha (HIF-1α), vascular endothelial cadherin (VE-Cad) and vascular endothelial growth factor A (VEGFA) in 1. blank liposomes; 2. dioscin liposomes; 3. epirubicin liposomes; 4. epirubicin and dioscin co-delivery liposomes; 5. RPV-modified epirubicin and dioscin co-delivery liposomes. (C-F,H) Semiquantitative analysis of MMP-2 (C), MMP-9 (D), HIF-1α (E), VE-Cad (F) and VEGFA (H). Protein expression was assessed by densitometry in A549 cells after treatment with the various liposomal formulations. Data are presented as mean ± SD (n = 6); (G) Inhibition of angiogenesis on chorioallantoic membrane (CAM). Scale bar, 5 mm. Comparison of a vs 1, b vs 2, c vs 3, d vs 4. Significance level was set at $P < .05$
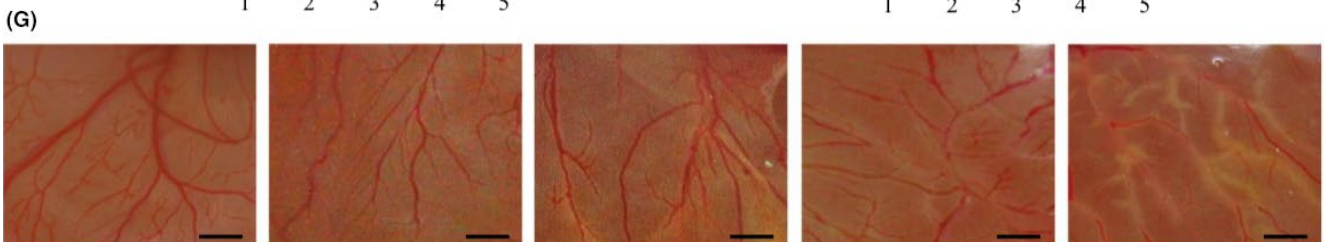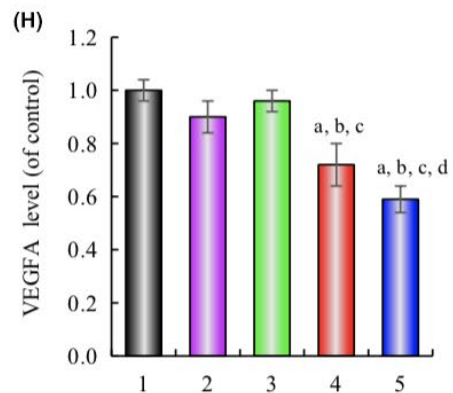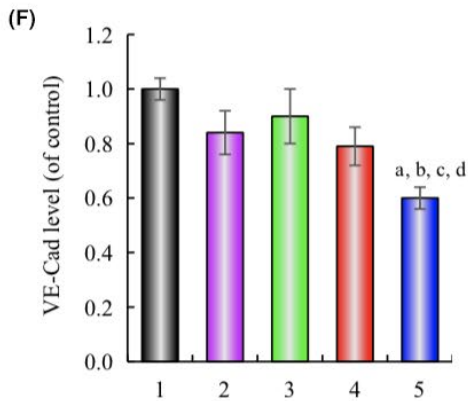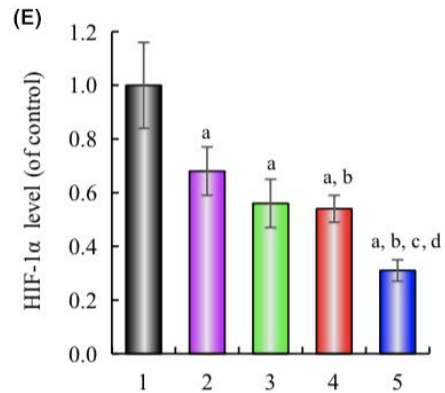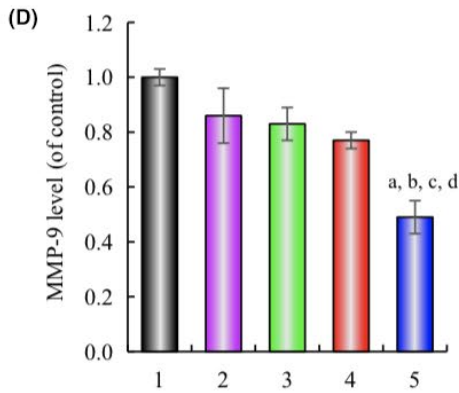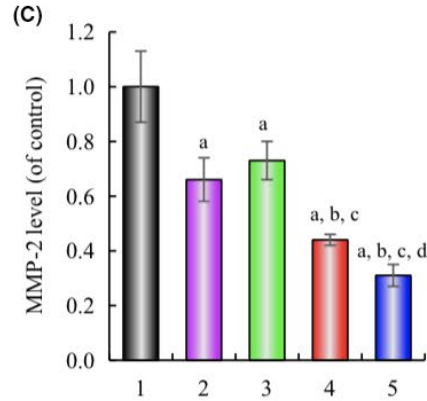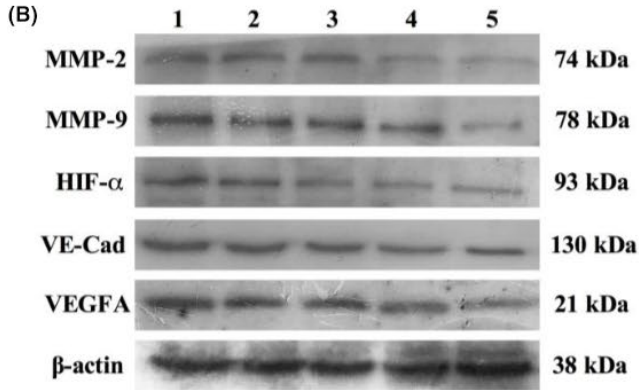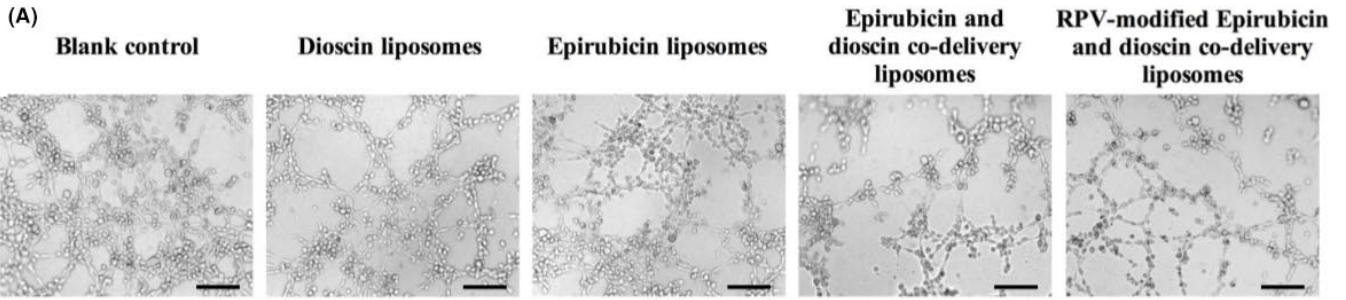
on VM channels. Furthermore, expression of VM-related proteins, including VE-Cad, HIF-1α, MMP-2, and MMP-9 was detected by western blot (Figure 5B-F). Expressions of all of these proteins decreased following treatment of the cells with various liposomal formulations, with RPV-modified epirubicin and dioscin co-delivery liposomes showing the strongest downregulation effect.

3.5 | Inhibition of angiogenesis

Chorioallantoic membrane (CAM) assay was used to evaluate the effect of the various liposomal formulations on angiogenesis (Figure 5G). As expected, blood vessels grew vigorously and density of new vessels increased when the membrane was incubated with culture medium. In contrast, density of new vessels decreased after treatment with the various drug formulations, with RPV-modified epirubicin and dioscin co-delivery liposomes showing the strongest inhibitory effect on CAM angiogenesis. VEGFA, an important mediator of angiogenesis during tumor development, is a member of the VEGF family.[37] Western blot analysis showed that VEGFA protein expression levels significantly decreased in CAM treated with epirubicin and dioscin co-delivery liposomes and RPV-modified epirubicin and dioscin co-delivery liposomes (Figure 5B,H).

3.6 | Inhibition of tumor cell invasion and migration

Effect of the various liposomal formulations on wound healing was studied (Figure 6A). When compared to the blank control, all drug-loaded liposomal formulations inhibited the repair of scratch wounds. Quantitative evaluation, using ImageJ software, showed that wound-healing inhibitory effect was in the following order: RPV-modified epirubicin and dioscin co-delivery liposomes >epirubicin and dioscin co-delivery liposomes >dioscin liposomes >epirubicin liposomes >blank control (Figure 6B). Transwell invasion assay was used to assess the effect of the various liposomal formulations on A549 cell migration. Results showed that dioscin-loaded liposomes caused a notable decrease in the number of invasive cells (Figure 6C). Among all liposomal formulations, RPV-modified epirubicin and dioscin co-delivery liposomes showed the strongest invasive and migratory inhibitory effect on A549 cells, with a relative migration rate of 14.91 ± 5.02% (Figure 6D), confirming our previous findings that dioscin plays a key role in inhibiting A549 cell invasion and migration.[33]

3.7 | Pharmacokinetics and biodistribution of epirubicin

Plasma concentration-time curves of epirubicin after treatment with the various liposomal formulations are shown in Figure S1. Results show that clearance of epirubicin from the blood circulation is rapid, and that free epirubicin was eliminated within 9 hours

after administration. In contrast, after treatment with the liposomal formulations, plasma concentration of epirubicin decreased slowly and remained at a higher concentration in the terminal phase. Pharmacokinetic parameters in vivo after giving the various liposomal formulations are presented in Table S1. Compared with free epirubicin, significantly prolonged elimination half-life ($t_{1/2}$), decreased clearance rate (CL) and increased area under the curve ($AUC_{0-24\ h}$) were observed following administration of various liposomal formulations. No significant differences were observed in plasma concentration of epirubicin or in the pharmacokinetic parameters among the various liposomal drug formulations.

Biodistribution details of the various formulations are presented in Figure S2. We found that the concentration of RPV-modified epirubicin-targeted liposomes was lower in the liver, spleen and kidneys, and higher in tumor tissue, when compared to epirubicin conventional liposomes and free epirubicin. Epirubicin concentration in tumor cells 6 hours after injection of RPV-modified epirubicin liposomes or RPV-modified epirubicin and dioscin co-delivery liposomes was, respectively, 75.92- and 77.69-fold higher than that for free epirubicin, 4.16- and 4.26-fold higher than that for epirubicin liposomes, and 4.52- and 4.63-fold higher than that for epirubicin and dioscin co-delivery liposomes.

3.8 | Fluorescence imaging in vivo

Representative images of tumor-bearing nude mice after giving the various formulations are presented in Figure 7. Results show that free DiR was mainly distributed in the liver for the duration of the experiment, and slight fluorescence signal was detected in tumor tissues. In contrast, strong fluorescence signals were observed in the tumor site after giving both DiR and RPV-modified DiR liposomes. Strong fluorescence signals in the RPV-modified treatment group were maintained for up to 48 hours. The elevated accumulation can be ascribed to the enhanced permeability and retention (EPR) effect and the interaction of RPV with tumor cells.

3.9 | Antitumor efficacy in tumor-bearing mice

To assess the antitumor effects of the various formulations in vivo, changes in body weight, relative tumor inhibiting rate, and tumor cell apoptosis were evaluated in treated tumor-bearing mice. As indicated in Figure 8A, no significant decrease in body weight of treatment groups was found when compared to the control group. All drug-treated groups showed different degrees of inhibition on tumor growth in comparison to the control group, with RPV-modified epirubicin and dioscin co-delivery liposomes showing the strongest tumor growth-inhibitory effect (Figure 8B). Morphological assessment by H&E staining indicated that RPV-modified epirubicin and dioscin co-delivery liposomes significantly disrupted the structure of tumor tissues and caused necrosis of tumor cells. Moreover,

to detect apoptotic cells in tumor tissues, a TUNEL assay was carried out. As shown in Figure 8C, number of apoptotic cells in the liposomal treatment groups was significantly higher than that in the free drug groups. RPV-modified epirubicin and dioscin co-delivery liposomes induced the largest number of apoptotic cells, indicating that it has the strongest inhibitory effect on tumor cell growth. Administration of the RPV-modified

epirubicin and dioscin co-delivery liposomes resulted in hematological parameters similar to the saline-treated group (Table S2). Histopathological analysis was done to examine the damage to major organs in the treated mice (Figure S3). No obvious organ damage was observed after giving the various formulations at the therapeutic dose used, indicating that the RPV-modified liposomes are safe and non-toxic.
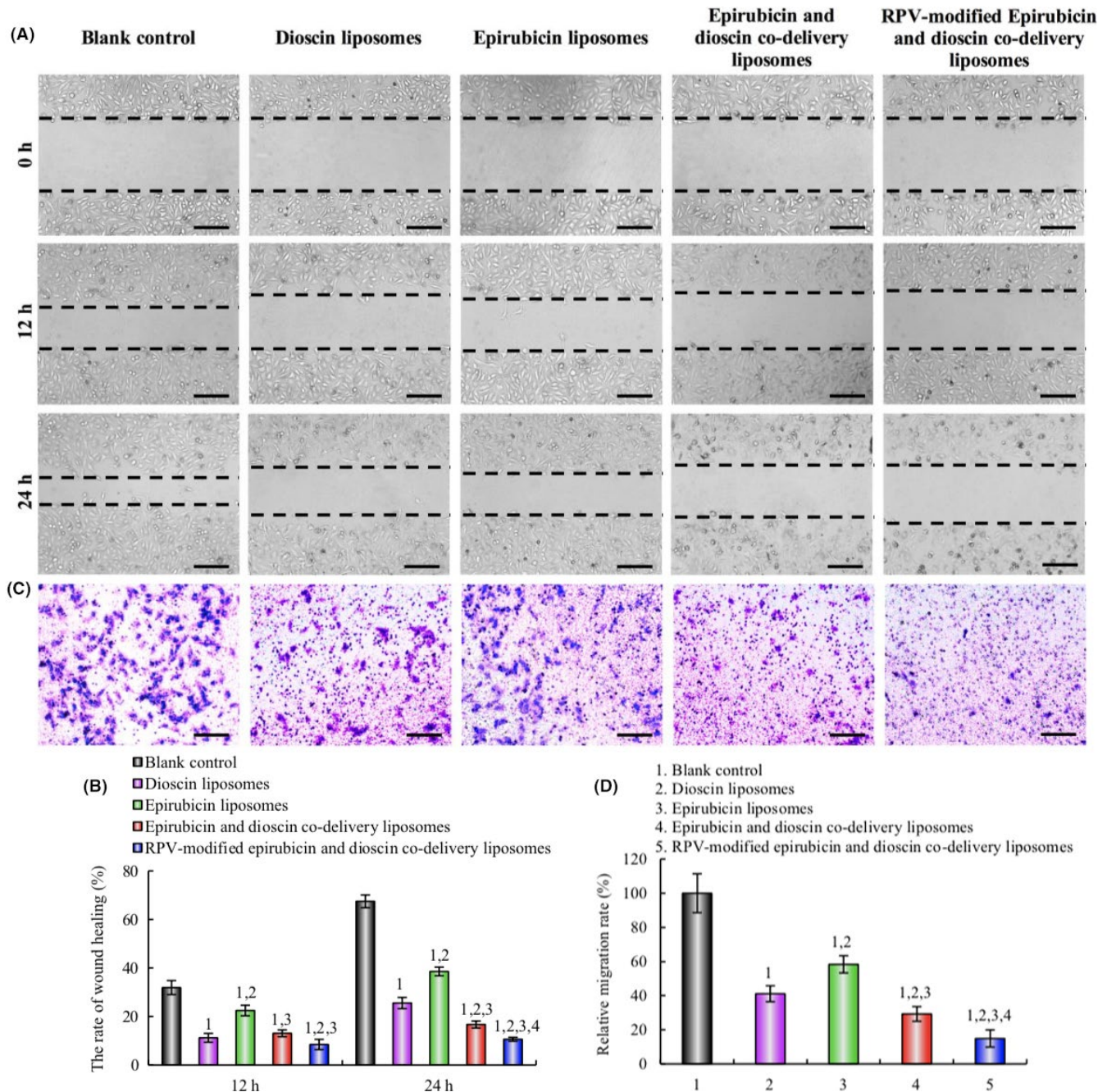
FIGURE 6 Inhibitory effects on invasion and migration of A549 cells after treatment with various liposomal formulations. A, Representative images of the extent of wound healing 12 h and 24 h after treatment with the various liposomal formulations. Scale bar, 50 μm. B, Quantitative analysis of wound healing rate in A549 cells after treatment with the various liposomal formulations. Data are presented as mean ± SD. C, Representative images of inhibition exerted on the ability of A549 cells to invade after treatment with the various liposomal formulations for 24 h. Scale bar, 50 μm. D, Semiquantitative analysis of relative invasion rate of A549 cells after treatment with the various liposomal formulations. Data are presented as mean ± SD (n = 6). Comparison of 1 vs blank control, 2 vs dioscin liposomes, 3 vs epirubicin liposomes, 4 vs epirubicin and dioscin co-delivery liposomes. Significance level was set at *P* < .05
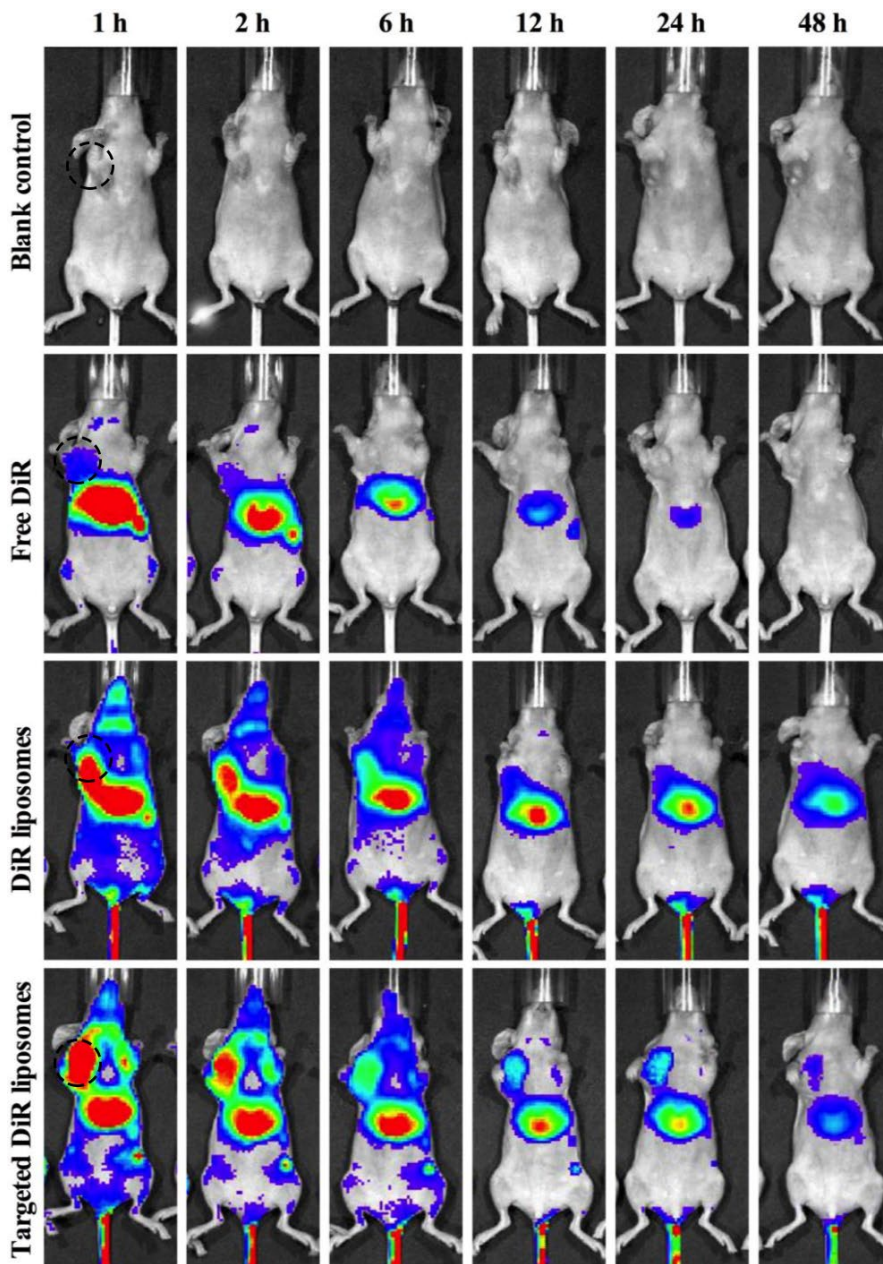
FIGURE 7 Real-time in vivo images after giving i.v. various liposomal formulations to tumor-bearing mice. Black dashed circles represent the location of tumor cell xenograft sites

3.10 | Inhibition of VM formation in vivo

To assess the effect of treatment on VM formation, tumors were stained with CD31/PAS double staining. Results showed VM structures with negative CD31 and positive PAS staining in tumors from the blank control group. Different degrees of VM structural damage and decreased VM quantity were observed in the various drug treatment groups. VM channels were small and thin after treatment with RPV-modified epirubicin and dioscin co-delivery liposomes, suggesting that the drug has a certain inhibitory effect on VM formation. Furthermore, key proteins of VM formation, including MMP-2, MMP-9, VEGFA, HIF-1α, and VE-Cad, could all be detected by immunofluorescence staining.[38] As shown in Figure 9B, blank control group showed the strongest fluorescence intensity. The relative fluorescence intensity of VM-related proteins decreased after treatment with the various

formulations. A semiquantitative evaluation by ImageJ software analysis showed that the relative fluorescence intensity rankings were: free epirubicin >free epirubicin plus dioscin >epirubicin liposomes >epirubicin and dioscin co-delivery liposomes >RPV-modified epirubicin and dioscin co-delivery liposomes. Clearly, RPV-modified epirubicin and dioscin co-delivery liposomes showed the strongest downregulation effect on VM-related proteins in tumor-bearing nude mice.

4 | DISCUSSION

Currently, surgery and chemotherapy are still the main treatment strategies for patients with NSCLC. Unfortunately, treatment outcome is usually unsatisfactory as a result of tumor metastasis and recurrence, as well as the severe systemic toxicity caused by the
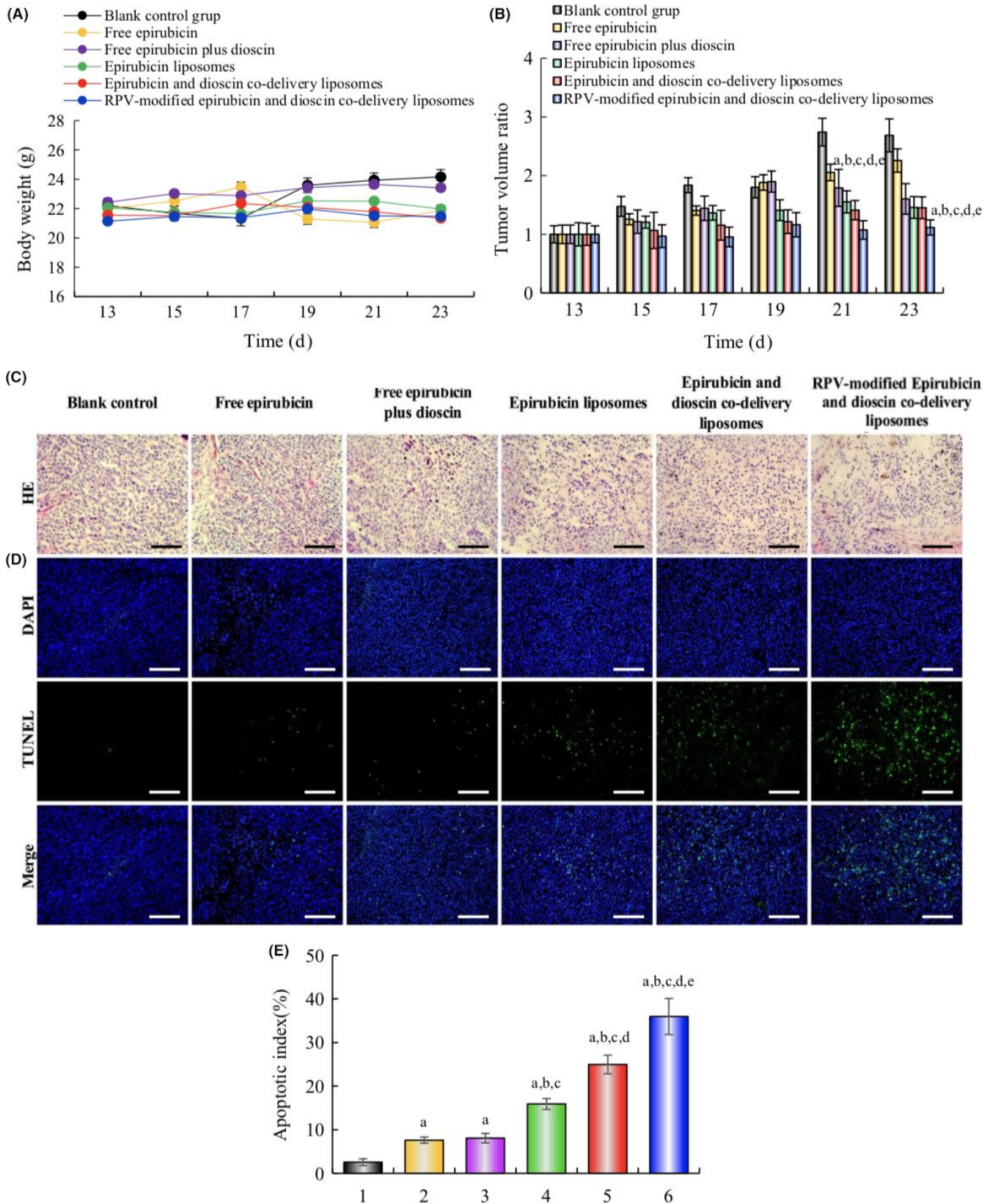
FIGURE 8 Antitumor efficacy in tumor-bearing mice after treatment with various liposomal formulations. A, Body weight alterations through the treatment process. B, Tumor volume changes during the treatment process. C, Representative images of pathological changes in tumor tissue by H&E staining. D, Representative images of apoptosis of tumor cells detected by TUNEL assay. Scale bar, 50 μm. E, Quantitative analysis of apoptotic index. 1. Blank control; 2. free epirubicin; 3. free epirubicin plus dioscin; 4. epirubicin liposomes; 5. epirubicin and dioscin co-delivery liposomes; 6. RPV-modified epirubicin and dioscin co-delivery liposomes. Data are presented as mean ± SD (n = 8). Comparison of a vs 1, b vs 2, c vs 3, d vs 4, e vs 5. Significance level was set at $P < .05$
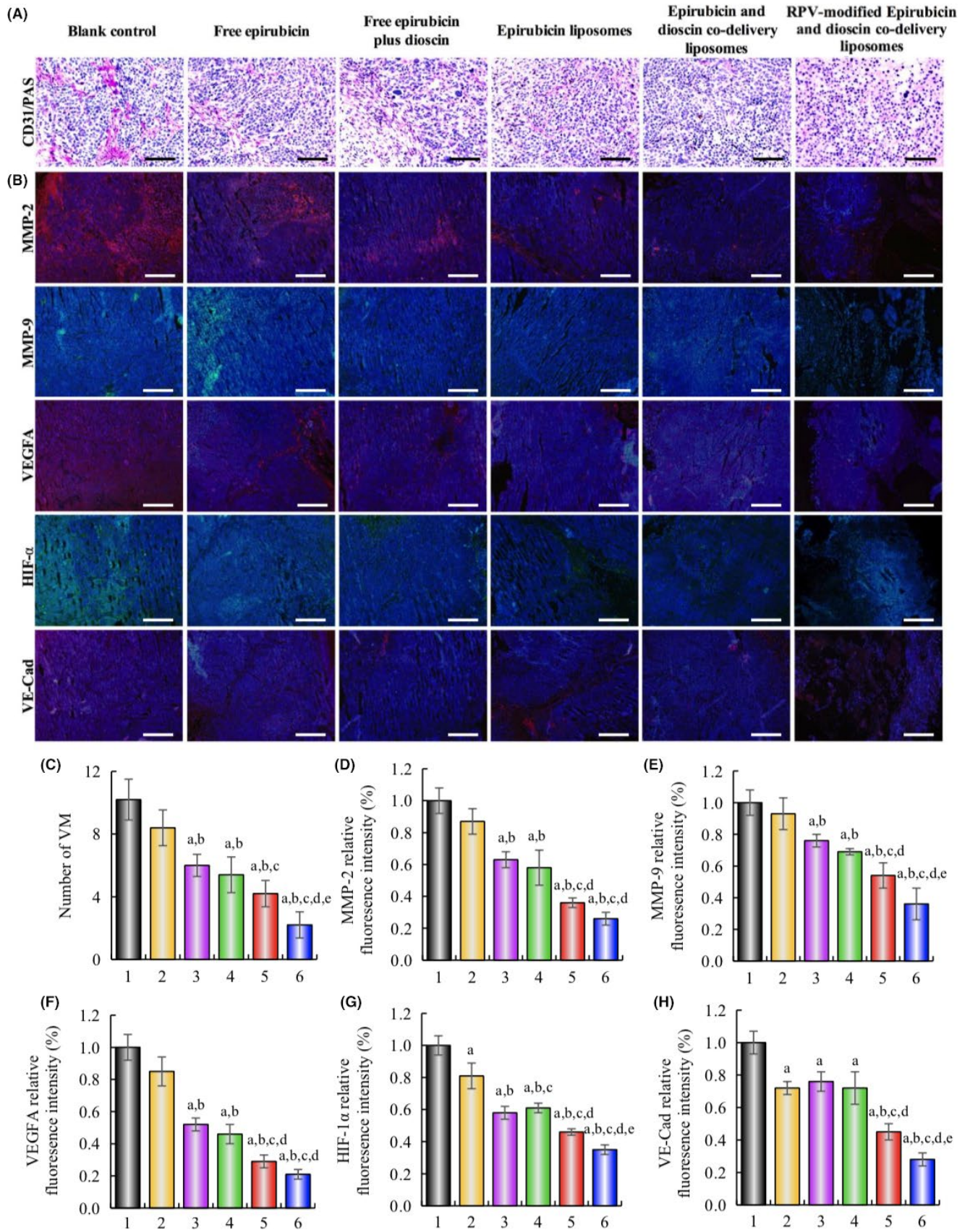
FIGURE 9 Inhibitory effects on vasculogenic mimicry (VM) channel formation and angiogenesis in tumor-bearing mice after treatment with various liposomal formulations. A, Representative images of VM channel formation in tumor tissue by CD31/PAS staining. Scale bar, 50 μm. B, Expression of MMP-2, MMP-9, vascular endothelial growth factor A (VEGFA), hypoxia-inducible factor 1 alpha (HIF-1α) and vascular endothelial cadherin (VE-Cad) detected by immunohistochemistry in tumor tissues. Scale bar, 50 μm. C, Quantitative analysis of the number of VM channels. (D-H) Semiquantitative analysis of MMP-2 (D), MMP-9 (E), VEGFA (F), HIF-1α (G) and VE-Cad (H) by relative fluorescence intensity in tumor tissues. Data are presented as mean ± SD (n = 8). 1. Blank control; 2. free epirubicin; 3. free epirubicin plus dioscin; 4. epirubicin liposomes; 5. epirubicin and dioscin co-delivery liposomes; 6. RPV-modified epirubicin and dioscin co-delivery liposomes. Comparison of a vs 1, b vs 2, c vs 3, d vs 4, e vs 5. Significance level was set at $P < .05$

poorly targeted chemotherapeutic drugs.[39,40] New drug-delivery strategies to improve treatment efficacy for NSCLC are therefore highly desirable. It is well known that nanoparticles, ranging in size between 20 and 200 nm, can easily penetrate into tumors and extend circulation time of their load.[41] Previous studies have shown that the dioscin suppresses growth of laryngeal cancer cells by inducing cell-cycle arrest and MAPK-mediated mitochondrial-derived apoptosis, and inhibiting tumor invasion and migration.[42-44] Furthermore, dioscin can inhibit the migration and invasion of A549 lung cancer cells by inhibiting TGF-β1 induction of epithelial-mesenchymal transition (EMT). Hence, to improve treatment of NSCLC, we developed RPV-modified epirubicin and dioscin co-delivery liposomes that showed increased active tumor targeting and inhibited tumor metastasis.

RPV is a novel small-molecule cell-penetrating peptide. In the present study, a DSPE-PEG$_{2000}$-RPV conjugate was successfully synthesized by acylation reaction as confirmed through MALDI-TOF-MS spectrum analysis (Figure 2A,B). The chemical and physical properties of the conjugate, including particle size, PDI, zeta potential values, and encapsulation efficiencies are important factors that determine its pharmacokinetics and biodistribution. Compared with the control liposomes, RPV-modified epirubicin and dioscin co-delivery liposomes were slightly larger in size as a result of the conjugation of DSPE-PEG$_{2000}$-RPV on the surface of the liposomes. Particle size of the targeted liposomes was approximately 100 nm, with a narrow PDI, which helped to enhance its accumulation in tumor tissue as a result of the EPR effect. The zeta potential values of all liposomal formulations were slightly negative due to the addition of DSPE-PEG$_{2000}$ (Table 1).

The therapeutic effect of drug-loaded liposomes is strongly influenced by drug accumulation inside tumor cells. Hence, cellular uptake is a critical factor for liposomal drug delivery systems.[45,46] Using flow cytometry and fluorescence microscopy, we showed that the fluorescence intensity of RPV-modified epirubicin and dioscin co-delivery liposomes was stronger than that of other liposomes, indicating that A549 cellular uptake of these liposomes was improved after being modified with RPV (Figure 3A-E). The increased cellular uptake in A549 cells could be explained by the interaction of the RPV peptide with the cellular membrane of tumor cells, facilitating increased delivery of the drugs into these cells. However, the highest uptake was found when free epirubicin was given. This might be due to diffusion of drug molecules through cellular membranes into the cells. When drug formulations were encapsulated in the liposomes, there was no direct drug-cell contact. Furthermore, particle size of liposomes was approximately 100 nm, much larger than the size of

the free drugs. This explained why the fluorescence intensity following their cellular uptake was weaker than that of free epirubicin.

CPPs depend on electrostatic interactions between positively charged sequences of amino acids (mainly basic amino acid residues rich in arginine and lysine) and negatively charged glycoproteins on the cell surface in physiological pH environments. The taurine group of arginine can form a hydrogen bond with the negatively charged phosphate and sulfuric acid groups on the surface of the cell membrane. Such bonding promotes cellular internalization, presumably the driving force behind penetration through the cellular membrane.[47] Herein, the intracellular distribution of targeting liposomes was observed by confocal laser scanning fluorescence microscopy. Red fluorescence signals on the surface of the cells suggested that the targeted epirubicin liposomes bind to the cellular membrane of tumor cells and are then transported into the cell and the nucleus. In contrast, epirubicin liposomes devoid of the RPV peptide showed weak ability to attach and cross cellular membranes. As expected, free epirubicin was diffusely distributed within the A549 cells.

The next challenge was to establish the link between good internalization mediated by RPV and subsequent cytotoxic effects on A549 cells. For this purpose, cell cytotoxicity assay was carried out.[48] Results indicated a synergetic cytotoxicity effect between epirubicin and dioscin, with dioscin alone showing a negligible effect on survival rate of A549 cells. We found that RPV-modified epirubicin and dioscin co-delivery liposomes had a significant inhibitory effect on the proliferation of A549 cells when compared with conventional liposomal formulation. An overall reduction in epirubicin IC$_{50}$ to 1.06 μmol/L was recorded. This further suggests that RPV modification and the existence of dioscin could increase active targeting and cytotoxicity of epirubicin-loaded liposomes on A549 cells.

Vasculogenic mimicry was discovered in invasive human melanoma by Maniotis and colleagues in 1999.[49] These researchers showed that VM is a special vascular structure in malignant tumors composed of highly invasive tumor cells. In the past decade, it was found that VM occurred in a variety of solid tumors, including NSCLC and hepatocellular carcinoma.[10,50] The presence of such pathological pseudo blood vessels in tumor tissue indicates poor patient prognosis. Studies have reported that the expression of HIF-1α was associated with VM channels, as well as with the growth and potential proliferation of tumor cells.[51] When oxygen supply is far less than the demand, tumor cells enter an anoxic state and then form VM channels. While in the hypoxic state, the enhanced HIF-1α induces the expression of VE-Cad, which mainly mediates cell-to-cell adhesion. HIF-1α also activates MMP and remodels the cellular matrix. The activated MMP degrade

the extracellular matrix, cleave laminin into multiple short chains, and facilitate the formation of VM channels.[16,52] In the present study, results showed that treatment with RPV-modified epirubicin and dioscin co-delivery liposomes severely disrupted the formation of VM channels in Matrigel, and significantly inhibited the expression of HIF-1α, VE-cadherin, MMP-2, and MMP-9 proteins. These results indicate that RPV-modified epirubicin and dioscin co-delivery liposomes could be used to limit tumor VM formation.

Tumor angiogenesis is a complex process comprising basement membrane degradation, endothelial cell proliferation and aggregation, and new tube formation.[53] In cancer, angiogenesis involves interaction between tumor cells, endothelial cells, and mesenchymal cells, which is orchestrated by growth factors or cytokines and their corresponding receptors. Among them, VEGFA plays a key role in the process of angiogenesis.[54] Recent studies have shown that a variety of cancer cells can upregulate the expression of VEGFA, thereby promoting tumor-induced angiogenesis.[55] With this in mind, we used the CAM assay to test the anti-angiogenic effect of liposomal formulations. This was further elaborated by evaluating VEGFA protein expression using western blot. As expected, we found that dioscin-loaded liposomes inhibited neovascularization and expression of VEGFA protein. Among the liposomal preparations, RPV-modified epirubicin and dioscin co-delivery liposomes showed the most obvious angiogenesis inhibitory effect.

It is necessary to investigate whether drug-loaded liposomes can inhibit lung cancer cell invasion and migration. In this study, a wound-healing assay was used to evaluate the inhibitory effect of the treatment on the invasiveness of A549 cells in vitro. Strong inhibition was observed after treatment with dioscin-loaded liposomes, suggesting that the addition of dioscin could significantly inhibit the invasiveness of A549 cells. We then used the Transwell migration assay to assess the ability of liposomal formulations to inhibit migration of A549 cells. Treatment with RPV-modified epirubicin and dioscin co-delivery liposomes resulted in the lowest number of penetrated cells, which further confirms that dioscin plays a key role in inhibiting A549 cell metastasis.

The plasma concentration-time curve of free epirubicin was compared with that of the liposomal formulations. Extended blood circulatory effects were achieved after PEGylation on the liposomal surface through avoidance of rapid uptake by the reticuloendothelial system (RES). Initially, the concentration of free epirubicin was significantly lower than that of the liposomal formulations. This can be explained by the rapid distribution of free epirubicin in the liver after administration via the tail vein. Furthermore, epirubicin liposomes showed better tumor-targeting ability, as indicated by drug accumulation in the tumors. To obtain real-time fluorescence images of drug-loaded liposomes in tumor-bearing mice, fluorescence DiR dye was encapsulated into the liposomal formulations. Imaging of tumor-bearing mice can indirectly reflect cycle time of the targeted molecule in vivo. More importantly, distribution of the various formulations at the same predetermined time points can be compared. Results show that

drug-loaded liposomes had extended stability in blood circulation, arising from the addition of DSPE-PEG$_{2000}$. RPV-modified DiR liposomes showed obvious accumulation in tumor sites, and the increased accumulation could be ascribed to the enhanced permeability and retention effects endowed by binding RPV to the surface of the liposomes. Consistent with the results on biodistribution analysis, RPV-modified DiR liposomes gained the potential to actively target NSCLC.

The inhibitory effect of various formulations on VM channels was also examined in vivo. Vasculogenic mimicry formation was detected in paraffin sections of tumor tissue by using CD31/PAS double staining. Tumor cells that had formed VM channels were negative for CD31, whereas endothelium-dependent blood vessels were positive for both CD31 and PAS.[56,57] Our results showed that RPV-modified epirubicin and dioscin co-delivery liposomes clearly inhibited VM formation in vivo. In support of this finding, we also detected strong in vivo downregulation of VM-related protein expression, including that of MMP-2, MMP-9, VEGFA, HIF-1α and VE-cadherin when tumor-bearing nude mice were treated with RPV-modified epirubicin and dioscin co-delivery liposomes.

In conclusion, we have shown that RPV-modified epirubicin and dioscin co-delivery liposomes could enhance antitumor efficacy in vitro and in vivo. This enhancement could be attributed to the following factors: (i) addition of hydrophilic materials prolonged circulation in the blood by slowing uptake through the reticuloendothelial system; (ii) binding of RPV on the liposomal surface enabled penetration through biological barriers and increased uptake of the drugs into A549 cells; (iii) incorporation of dioscin augmented overall antitumor efficacy by inhibiting tumor angiogenesis, VM channel formation, migration and invasion. We believe that RPV-modified epirubicin and dioscin co-delivery liposomes could be a promising approach to the treatment of NSCLC.

ORCID

Xue-tao Li 🆔 https://orcid.org/0000-0002-0608-4669

REFERENCES

1. Gantenbein N, Bernhart E, Anders I, et al. Influence of eukaryotic translation initiation factor 6 on non-small cell lung cancer development and progression. *Eur J Cancer*. 2018;101:165-180.
2. Tane S, Sakai Y, Hokka D, et al. Significant role of Psf3 expression in non-small-cell lung cancer. *Cancer Sci*. 2015;106(11):1625-1634.
3. Najlah M, Ahmed Z, Iqbal M, et al. Development and characterisation of disulfiram-loaded PLGA nanoparticles for the treatment of non-small cell lung cancer. *Eur J Pharm Biopharm*. 2017;112:224-233.

4. Liu JJ, Tang W, Fu M, et al. Development of R8 modified Epirubicin-dihydroartemisinin liposomes for treatment of non-small-cell lung cancer. *Artif Cells Nanomed Biotechnol*. 2019;47:1947-1960.

5. Shi S, Luo W, Zhang R, et al. CRTC2 promotes non-small cell lung cancer A549 migration and invasion in vitro. *Thoracic cancer*. 2018;9:136-141.

6. Di Leo N, Battaglini M, Berger L, et al. A catechin nanoformulation inhibits WM266 melanoma cell proliferation, migration and associated neo-angiogenesis. *Eur J Pharm Biopharm*. 2017;114:1-10.

7. Han L, Wang JN, Cao XQ, Sun CX, Du X. An-te-xiao capsule inhibits tumor growth in non-small cell lung cancer by targeting angiogenesis. *Biomed Pharmacother*. 2018;108:941-951.

8. Mao G, Liu Y, Fang X, et al. Tumor-derived microRNA-494 promotes angiogenesis in non-small cell lung cancer. *Angiogenesis*. 2015;18:373-382.

9. Kawahara R, Niwa Y, Simizu S. Integrin β1 is an essential factor in vasculogenic mimicry of human cancer cells. *Cancer Sci*. 2018;109:2490–2496.

10. Williamson SC, Metcalf RL, Trapani F, et al. Vasculogenic mimicry in small cell lung cancer. *Nat Commun*. 2016;7:13322.

11. Wang S, Zhang Z, Qian W, et al. Angiogenesis and vasculogenic mimicry are inhibited by 8-Br-cAMP through activation of the cAMP/PKA pathway in colorectal cancer. *Onco Targets Ther*. 2018;11:3765-3774.

12. Hulin JA, Tommasi S, Elliot D, Mangoni AA. Small molecule inhibition of DDAH1 significantly attenuates triple negative breast cancer cell vasculogenic mimicry in vitro. *Biomed Pharmacother*. 2019;111:602-612.

13. Lin X, Sun R, Zhao X, et al. C-myc overexpression drives melanoma metastasis by promoting vasculogenic mimicry via c-myc/snail/Bax signaling. *J Mol Med*. 2017;95:53-67.

14. Wang W, Lin P, Sun B, et al. Epithelial-mesenchymal transition regulated by EphA2 contributes to vasculogenic mimicry formation of head and neck squamous cell carcinoma. *Biomed Res Int*. 2014;2014:803914.

15. Li S, Zhang Q, Zhou L, et al. Inhibitory effects of compound DMBT on hypoxia-induced vasculogenic mimicry in human breast cancer. *Biomed Pharmacother*. 2017;96:982-992.

16. Yeo C, Lee H-J, Lee E-O. Serum promotes vasculogenic mimicry through the EphA2/VE-cadherin/AKT pathway in PC-3 human prostate cancer cells. *Life Sci*. 2019;221:267-273.

17. Wang Y, Tong L, Wang J, et al. cRGD-functionalized nanoparticles for combination therapy of anti-endothelium dependent vessels and anti-vasculogenic mimicry to inhibit the proliferation of ovarian cancer. *Acta Biomater*. 2019;94:495-504.

18. Taghdisi SM, Danesh NM, Ramezani M, et al. Double targeting and aptamer-assisted controlled release delivery of Epirubicin to cancer cells by aptamers-based dendrimer in vitro and in vivo. *Eur J Pharm Biopharm*. 2016;102:152-158.

19. Wang H, Zhang Y, Yang H, et al. In vivo SELEX of an inhibitory NSCLC-specific RNA aptamer from PEGylated RNA library. *Mol Ther Nucleic Acids*. 2018;10:187-198.

20. Ikeda M, Kudo M, Aikata H, et al. Transarterial chemoembolization with miriplatin vs. Epirubicin for unresectable hepatocellular carcinoma: a phase III randomized trial. *J Gastroenterol*. 2017;53:281-290.

21. Song XL, Ju RJ, Xiao Y, et al. Application of multifunctional targeting Epirubicin liposomes in the treatment of non-small-cell lung cancer. *Int J Nanomed*. 2017;12:7433-7451.

22. Ju RJ, Cheng L, Xiao Y, et al. PTD modified paclitaxel anti-resistant liposomes for treatment of drug-resistant non-small cell lung cancer. *J Liposome Res*. 2018;28:236-248.

23. Cheng L, Huang FZ, Cheng LF, et al. GE11-modified liposomes for non-small cell lung cancer targeting: preparation, ex vitro and in vivo evaluation. *Int J Nanomed*. 2014;9:921-935.

24. Tang YN, Pang YX, He XC, et al. UPLC-QTOF-MS identification of metabolites in rat biosamples after oral administration of Dioscorea saponins: a comparative study. *J Ethnopharmacol*. 2015;165:127-140.

25. Tao X, Yin L, Xu L, Peng J. Dioscin: A diverse acting natural compound with therapeutic potential in metabolic diseases, cancer, inflammation and infections. *Pharmacol Res*. 2018;137:259-269.

26. Zheng L, Han X, Hu Y, et al. Dioscin ameliorates intestinal ischemia/reperfusion injury via adjusting miR-351-5p/MAPK13-mediated inflammation and apoptosis. *Pharmacol Res*. 2019;139:431-439.

27. Kim EA, Jang JH, Lee YH, et al. Dioscin induces caspase-independent apoptosis through activation of apoptosis-inducing factor in breast cancer cells. *Apoptosis*. 2014;19:1165-1175.

28. Lim WC, Kim H, Kim YJ, et al. Dioscin suppresses TGF-beta1-induced epithelial-mesenchymal transition and suppresses A549 lung cancer migration and invasion. *Bioorg Med Chem Lett*. 2017;27:3342-3348.

29. Si L, Zheng L, Xu L, et al. Dioscin suppresses human laryngeal cancer cells growth via induction of cell-cycle arrest and MAPK-mediated mitochondrial-derived apoptosis and inhibition of tumor invasion. *Eur J Pharmacol*. 2016;774:105-117.

30. Lee D, Noh I, Yoo J, Rejinold NS, Kim YC. pH-controllable cell-penetrating polypeptide that exhibits cancer targeting. *Acta Biomater*. 2017;57:187-196.

31. Qiu Y, Yu Q, Liu Y, et al. Dual receptor targeting cell penetrating peptide modified liposome for glioma and breast cancer postoperative recurrence therapy. *Pharm Res*. 2018;35:130.

32. Shi K, Li J, Cao Z, et al. A pH-responsive cell-penetrating peptide-modified liposomes with active recognizing of integrin alphavbeta3 for the treatment of melanoma. *J Control Release*. 2015;217:138-150.

33. Wang Y, Fu M, Liu J, et al. Inhibition of tumor metastasis by targeted daunorubicin and dioscin codelivery liposomes modified with PFV for the treatment of non-small-cell lung cancer. *Int J Nanomed*. 2019;14:4071-4090.

34. Li XT, Tang W, Xie HJ, et al. The efficacy of RGD modified liposomes loaded with vinorelbine plus tetrandrine in treating resistant brain glioma. *J Liposome Res*. 2019;29:21-34.

35. Ju RJ, Cheng L, Peng XM, et al. Octreotide-modified liposomes containing daunorubicin and dihydroartemisinin for treatment of invasive breast cancer. *Artif Cells Nanomed Biotechnol*. 2018;46:616-628.

36. Wang X, Cheng L, Xie HJ, et al. Functional paclitaxel plus honokiol micelles destroying tumour metastasis in treatment of non-small-cell lung cancer. *Artif Cells Nanomed Biotechnol*. 2018;46:1154-1169.

37. Tan Z, Chen K, Wu W, et al. Overexpression of HOXC10 promotes angiogenesis in human glioma via interaction with PRMT5 and upregulation of VEGFA expression. *Theranostics*. 2018;8:5143-5158.

38. Guo JQ, Zheng QH, Chen H, et al. Ginsenoside Rg3 inhibition of vasculogenic mimicry in pancreatic cancer through downregulation of VEcadherin/EphA2/MMP9/MMP2 expression. *Int J Oncol*. 2014;45:1065-1072.

39. Schaal CM, Bora-Singhal N, Kumar DM, Chellappan SP. Regulation of Sox2 and stemness by nicotine and electronic-cigarettes in non-small cell lung cancer. *Mol Cancer*. 2018;17:149.

40. Nascimento AV, Singh A, Bousbaa H, Ferreira D, Sarmento B, Amiji MM. Overcoming cisplatin resistance in non-small cell lung cancer with Mad2 silencing siRNA delivered systemically using EGFR-targeted chitosan nanoparticles. *Acta Biomater*. 2017;47:71-80.

41. Bertucci A, Kim KH, Kang J, et al. Tumor-targeting, microRNA-silencing porous silicon nanoparticles for ovarian cancer therapy. *ACS Appl Mater Interfaces*. 2019;11:23926-23937.

42. Guo X, Ding X. Dioscin suppresses the viability of ovarian cancer cells by regulating the VEGFR2 and PI3K/AKT/MAPK signaling pathways. *Oncol Lett*. 2018;15:9537-9542.

43. Hsieh M-J, Tsai T-L, Hsieh Y-S, Wang C-J, Chiou H-L. Erratum to: Dioscin-induced autophagy mitigates cell apoptosis through modulation of PI3K/Akt and ERK and JNK signaling pathways in human lung cancer cell lines. *Arch Toxicol*. 2017;91:2495-2496.

44. Tong Q, Qing Y, Wu Y, Hu X, Jiang L, Wu X. Dioscin inhibits colon tumor growth and tumor angiogenesis through regulating VEGFR2 and AKT/MAPK signaling pathways. *Toxicol Appl Pharmacol*. 2014;281:166-173.

45. Li J, Cheng X, Chen Y, et al. Vitamin E TPGS modified liposomes enhance cellular uptake and targeted delivery of luteolin: An in vivo/in vitro evaluation. *Int J Pharm*. 2016;512:262-272.

46. Na K, Lee SA, Jung SH, Hyun J, Shin BC. Elastin-like polypeptide modified liposomes for enhancing cellular uptake into tumor cells. *Colloids Surf B Biointerfaces*. 2012;91:130-136.

47. Takechiharaya Y, Saito H. Current understanding of physicochemical mechanisms for cell membrane penetration of arginine-rich cell penetrating peptides: role of glycosaminoglycan interactions. *Curr Protein Pept Sci*. 2018;19(6):623-630.

48. Deshpande P, Jhaveri A, Pattni B, Biswas S, Torchilin V. Transferrin and octaarginine modified dual-functional liposomes with improved cancer cell targeting and enhanced intracellular delivery for the treatment of ovarian cancer. *Drug Delivery*. 2018;25:517-532.

49. Maniotis AJ, Folberg R, Hess A, et al. Vascular channel formation by human melanoma cells in vivo and in vitro: vasculogenic mimicry. *Am J Pathol*. 1999;155(3):739–752.

50. Zhao X, Sun B, Liu T, et al. Long noncoding RNA n339260 promotes vasculogenic mimicry and cancer stem cell development in hepatocellular carcinoma. *Cancer Sci*. 2018;109:3197-3208.

51. Chen Q, Lin W, Yin Z, et al. Melittin inhibits hypoxia-induced vasculogenic mimicry formation and epithelial-mesenchymal transition through suppression of HIF-1alpha/Akt pathway in liver cancer. *Evid Based Complement Alternat Med*. 2019;2019:9602935.

52. Xia Y, Cai XY, Fan JQ, et al. The role of sema4D in vasculogenic mimicry formation in non-small cell lung cancer and the underlying mechanisms. *Int J Cancer*. 2019;144:2227-2238.

53. Hu J, Cheng Y, Li Y, et al. microRNA-128 plays a critical role in human non-small cell lung cancer tumourigenesis, angiogenesis and lymphangiogenesis by directly targeting vascular endothelial growth factor-C. *Eur J Cancer*. 2014;50:2336-2350.

54. Song F, Chen Q, Rao W, et al. OVA66 promotes tumour angiogenesis and progression through enhancing autocrine VEGF-VEGFR2 signalling. *EBioMedicine*. 2019;41:156-166.

55. Sun H, Zhang D, Yao Z, et al. Anti-angiogenic treatment promotes triple-negative breast cancer invasion via vasculogenic mimicry. *Cancer Biol Ther*. 2017;18:205-213.

56. Yao L, Zhang D, Zhao X, et al. Dickkopf-1-promoted vasculogenic mimicry in non-small cell lung cancer is associated with EMT and development of a cancer stem-like cell phenotype. *J Cell Mol Med*. 2016;20:1673-1685.

57. Stenzel M, Tura A, Nassar K, et al. Analysis of caveolin-1 and phosphoinositol-3 kinase expression in primary uveal melanomas. *Clin Exp Ophthalmol*. 2016;44:400-409.

SUPPORTING INFORMATION

Additional supporting information may be found online in the Supporting Information section.